Korean J. Chem. Eng., 32(3), 521-533 (2015)
DOI: 10.1007/s11814-014-0364-0

pISSN: 0256-1115
eISSN: 1975-7220

High-pressure solubility of carbon dioxide in pyrrolidinium-based ionic liquids: [bmpyr][dca] and [bmpyr][Tf_2N]

Byung-Chul Lee† and Sang Gyu Nam

Department of Chemical Engineering, Hannam University, 1646, Yuseong-daero, Yuseong-gu, Daejeon 305-811, Korea
(*Received 3 November 2014 • accepted 5 December 2014*)

Abstract−Solubility data of carbon dioxide (CO_2) in two pyrrolidinium-based ionic liquids: 1-butyl-1-methylpyrrolidinium dicyanamide ([bmpyr][dca]) and 1-butyl-1-methylpyrrolidinium bis(trifluoromethylsulfonyl)imide ([bmpyr][Tf_2N]) are presented at pressures up to about 30 MPa and temperatures from 303.2 K to 343.2 K. The solubility was determined by measuring bubble or cloud point pressures of mixtures of CO_2 and ionic liquid using a high-pressure equilibrium apparatus equipped with a variable-volume view cell. The CO_2 solubility in the ionic liquid in terms of the mole fraction or the molality increased with the increase of the equilibrium pressure at a given temperature, but decreased with the increase of temperature at a given pressure. At a given temperature, the mole fraction of CO_2 dissolved in the ionic liquid increased rapidly as pressure increased. CO_2 solubility in the mole fraction almost reached saturation around 0.65 for [bmpyr][dca] and around 0.8 for [bmpyr][Tf_2N], respectively. The experimental data for the CO_2+ ionic liquid systems were correlated using the Peng-Robinson equation of state (PR-EoS). The mixing rules of the Wong-Sandler type rather than the classical mixing rules of the van der Waals type were coupled with the PR-EoS. The resulting modeling approach proved to be able to correlate the CO_2 solubilities in aforementioned ionic liquids over the aforementioned range of temperature and pressure within 5% average deviations.

Keywords: Solubility, Carbon Dioxide (CO_2), Ionic Liquid, Pyrrolidinium, Correlation, Peng-Robinson Equation of State, Wong-Sandler Mixing Rules

INTRODUCTION

The suspected correlation between the increased carbon dioxide (CO_2) concentration in the atmosphere and the green-house effect has initiated a worldwide debate aimed at emission reduction of CO_2 and other green-house gases [1]. CO_2 emissions have increased since the dawn of the industrial revolution. This resulted in an increase of CO_2 concentration in the atmosphere from about 280 ppm before the industrialization to 390 ppm nowadays [1]. Currently, the power sector is responsible for 41% of all the energy-related CO_2 emissions, followed by the transport sector (23%), industry sector (20%), buildings sector (10%), and others [1]. The high share of the CO_2 emission in the power sector is related to fuel combustion to generate electricity or heat. CO_2 emission will continue to increase and will most likely double, relative to the 2007 emission of 28.8 Gt, by 2050 [1]. In the long term, a transition in energy path, from fossil fuels to low-carbon-technologies, will be required. However, in the foreseeable future, fossil fuel will continue to be a substantial fraction of the energy portfolio. In this regard CO_2 capture and storage (CCS) will be essential [2], although it should be considered as a temporary solution to the problem. Both, the capture of CO_2 and the storage are technical challenging and many hurdles have to be overcome to commercialize these processes [2,3].

The major barrier to commercialize the CCS process at large scale is the energy/cost associated with the separation method. Among the various avenues available for efficient CO_2 removal, absorption in aqueous amine solutions has long been proven and has been most effective so far [4]. However, the capture of CO_2 with amine solutions involves a chemical reaction with a large enthalpy of reaction [5]. Consequently, a large amount of heat is required to release the captured CO_2 in the regeneration step. Besides, the amine-based methods have several concerns including high volatility, thermal instability, corrosion, and degradation of amines. Those concerns have driven researchers to look for new and alternative technologies.

Recently, room temperature ionic liquids, called green solvents, are emerging as promising candidates to capture CO_2 due to their wide liquid range, extremely low volatility (namely, almost immeasurable vapor pressure), and reasonable thermal stability [6-8]. Moreover, CO_2 has shown to be highly soluble in ionic liquids. The low volatility of ionic liquids would not cause any contamination to a gas stream, and thus this feature gives ionic liquids a big advantage over conventional solvents used for absorbing CO_2. The ionic liquid has a feature of the physical absorbent in which CO_2 absorption capacity increases with increasing pressure. Therefore, it is advantageous to the pre-combustion CO_2 capture process, which absorbs CO_2 at a high-pressure (2-6 MPa) and release CO_2 at a low-pressure. The use of the ionic liquid as an absorbent for CO_2 can greatly reduce separation cost, since the energy consumption in the CO_2 separation step is small.

†To whom correspondence should be addressed.
E-mail: bclee@hannam.kr
‡This paper is dedicated to Prof. Hwayong Kim in commemoration of his retirement from the School of Chemical and Biological Engineering of Seoul National University.

Table 1. Ionic liquids studied in this work

Chemical name	Abbreviation	Chemical formula	CAS number	Molecular mass	Purity (mass %)	Water content (mass %)
1-Butyl-1-methylpyrrolidinium dicyanamide	[bmpyr][dca]	$C_{11}H_{20}N_4$	370865-80-8	208.30	≥97.0	0.57
1-Butyl-1-methylpyrrolidinium bis(trifluoromethylsulfonyl)imide	[bmpyr][Tf_2N]	$C_{11}H_{20}N_2S_2O_4F_6$	223437-11-4	648.85	≥98.5	0.16

To find the most suitable ionic liquid as an absorption solvent for CO_2 requires a precise knowledge of the CO_2 solubility in the ionic liquid. The rational design of the corresponding absorption system suitable for industrial scale-up purposes will require a precise knowledge of the physical equilibrium between CO_2 and the ionic liquid. A vast number of experimental works in the literature deal with CO_2 solubility in various kinds of ionic liquids at different temperature and pressure conditions [9-27].

In this work, we measured the CO_2 solubilities for two kinds of pyrrolidinium cation-based ionic liquids with different anions: butylmethylpyrrolidinium dycianamide ([bmpyr][dca]) and butylmethylpyrrolidinium bis(trifluoromethylsulfonyl)imide ([bmpyr][Tf_2N]). A high-pressure phase equilibrium measuring equipment with a variable-volume view cell was used as an experimental apparatus. The solubility was determined on the basis of measuring phase boundaries: bubble point pressures, for a mixture of CO_2 and ionic liquid with a known composition at a fixed temperature. From the phase boundary data of the binary mixture, the CO_2 solubilities were obtained as a function of temperature and pressure.

Since experimental measurements of phase equilibrium of ionic liquids and their mixtures may often become expensive and time consuming, it is highly desirable to have thermodynamic models for estimating CO_2 solubilities in ionic liquids that are valid within the operating conditions of the absorption system. Actually, various modeling efforts have been reported in the literature regarding the gas solubility in ionic liquids [28-33]. Vega et al. [34] published a comprehensive review on the state-of-the-art approaches for modeling the thermo-physical properties of ionic liquids including their gas solubilities. Among various types of modeling approaches, a cubic equation of state model is preferred, because it is the simplest approach to modeling the phase behavior of fluid mixture and furthermore it is always available in process simulators. Another objective of this study is to present a modeling approach of the CO_2 solubility in the aforementioned ionic liquids by the use of the Peng-Robinson equation of state (PR-EoS), which is one of the most popular cubic equations of state. So the mixing rules of the Wong-Sandler type rather than the classical mixing rules of the van der Waals type were coupled with the PR-EoS.

EXPERIMENTAL

1. Materials

The two ionic liquids ([bmpyr][dca] and [bmpyr][Tf_2N]) used in this work were purchased from Sigma-Aldrich Co. For solubility measurements, the ionic liquid sample was placed in the equilibrium cell followed by evacuation using a mechanical pump at room temperature during several days. The analysis of Coulometric Karl Fischer titration (Metrohm model 684) was performed to measure the water content for the evacuated ionic liquid samples. The characteristic values of the ionic liquids studied in this work are given in Table 1, and their chemical structures in Fig. 1. Information on the purity of ionic liquids was provided by the supplier. CO_2 with 99.99% high purity to be used for measurements was purchased from Myung Sin General Gas Co. (Korea). No further purification was performed for use of the ionic liquids and CO_2.

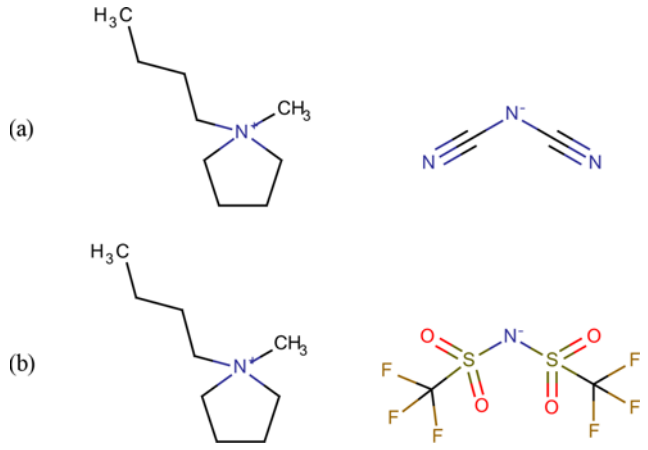

Fig. 1. Chemical structures of ionic liquids studied in this work: (a) [bmpyr][dca]; (b) [bmpyr][Tf_2N].

2. Apparatus and Procedure

A high-pressure variable-volume view cell apparatus was set up for measuring the solubility of CO_2 in ionic liquids. A schematic diagram of the experimental apparatus and a detailed description of the experimental procedure are given in our previous publications [12,13,22-24,27]. The apparatus has a view cell equipped with a sapphire window and a movable piston, a pressure generator (High Pressure Equipment Co. model 50-6-15), a borescope (Olympus model R080-044-000-50), a magnetic stirring system, and an air bath. The cylindrical view cell is 16 mm i.d. by 70 mm o.d., and its internal working volume is approximately 31 cm^3. A high-precision pressure gauge (Dresser Heise model CC-12-G-A-02B, ±0.05 MPa accuracy, ±0.01 MPa resolution) was used to measure the system pressure. An RTD probe inserted into the cell was used in measurement of the system temperature within ±0.1 K.

CO_2 solubilities in ionic liquid were determined through measuring bubble point pressures for CO_2+ionic liquid mixtures with various compositions at known temperatures. One feature of using the variable-volume view cell apparatus is that the concentration of the system is maintained constant throughout the experiment. A brief description of the experimental procedure is as follows. An

ionic liquid sample was injected into the cell by using a gas-tight syringe. A sensitive balance (AND model HM-30) measurable to ±0.1 mg was used in determining the amount of the ionic liquid loaded. The cell was placed within the air bath after a piston and a sapphire window were assembled. Then the cell was evacuated with a mechanical pump at room temperature during overnight to remove any entrapped air inside the cell and any dissolved gas and water in the ionic liquid.

CO_2 was delivered to the cell via a feed line by a small CO_2 cylinder after the vapor space of the cell was fully evacuated. The exact amount of CO_2 delivered to the cell was determined by measuring the weights of the CO_2 cylinder before and after delivery, with a balance (Precisa model 1212 M) with an accuracy of ±1 mg. Through dipping the CO_2 cylinder in a Dewar flask full of liquid nitrogen, CO_2 gas in the feed line was recovered back into the CO_2 cylinder. For ionic liquid and CO_2, uncertainties in measuring their masses were 0.2 mg and 2 mg, respectively. For the composition of each component, an uncertainty analysis was performed according to the ISO guideline [35].

For a CO_2+ionic liquid mixture with a specified overall composition, the system pressure was changed until the phase change inside the cell was visually observed through the cell window. The fluid in the cell was compressed to dissolve CO_2 into the ionic liquid. The fluid was well stirred and simultaneously heated to the target temperature. The system temperature was controlled within an uncertainty of ±0.1 K. At an elevated pressure, the fluid became a single homogeneous phase after dissolution of CO_2 into the ionic liquid phase. Then the pressure slowly decreased until tiny CO_2 bubbles started to form from the single phase solution. We defined the bubble point pressure of the solution at a given composition and temperature to be the initial pressure at which the first bubbles were observed. Every observation was repeated at least twice to ensure the reproducibility of experimental data. The uncertainty in measuring the bubble point pressure was 0.02 MPa. For a solution of very high CO_2 mole fractions, the cloud point behavior rather than the bubble point behavior was observed. Due to the phase transition from a single phase to a liquid+liquid phase, the solution became cloudy at the cloud point. The cloud pressure was defined to be the pressure at which there was no more possibility of visually observing the stirring bar in the cell [36]. The precision for the measurement of cloud pressure was estimated to be about 0.1 MPa. Exactly the same approach was repeated to measure the bubble or cloud point pressures at different temperatures and compositions.

CORRELATION

The solubility data for the binary systems obtained in this work were correlated with a thermodynamic model which can be incorporated into a mathematical model for design calculation of absorption column. The use of the thermodynamic model normally includes binary interaction parameters, which must be determined using experimental data for the binary systems. The correlation starts with a set-up of phase equilibrium criterion for a binary system of CO_2 (component 1)+ionic liquid (component 2). Only pure CO_2 exists in the gas phase, because the ionic liquid is taken to be non-volatile. Thus, the phase equilibrium condition is satisfied when the fugacities of CO_2 have equal values in both phases at a constant temperature and pressure:

$$f_1^{gas} = \hat{f}_1^{IL} \quad \text{or} \quad \phi_1^{gas} = \hat{\phi}_1^{IL} x_1 \tag{1}$$

where f_1^{gas} is the fugacity of CO_2 in pure gas phase and $\hat{f}_1^{IL}$ is the fugacity of CO_2 in ionic liquid phase. ϕ_1^{gas} and $\hat{\phi}_1^{IL}$ are the fugacity coefficients of CO_2 in pure gas phase and in ionic liquid phase, respectively, and x_1 is the composition (mole fraction) of CO_2 in ionic liquid phase. When the fugacity coefficient is used in both phases, the method of solution of the phase equilibrium problem is known as the equation of state (EoS) method. Then, an EoS and a set of mixing rules are needed, to express the fugacity coefficient as functions of temperature, pressure and composition [37,38]. Among a variety of the EoS, the Peng-Robinson equation of state (PR-EoS), one of the most popular for practical applications, was used in this work. The PR-EoS has been proven to combine the simplicity and accuracy required for the prediction and correlation of volumetric and thermodynamic properties of fluids.

The PR-EoS is written as follows [37]:

$$P = \frac{RT}{V-b} - \frac{a(T)}{V(V+b)+b(V-b)} \tag{2}$$

with

$$a(T) = 0.457235 \frac{R^2 T_c^2}{P_c} \alpha(T_r) \tag{3}$$

$$b = 0.077796 \frac{RT_c}{P_c} \tag{4}$$

$$\alpha(T_r) = [1 + (0.37464 + 1.54226\omega - 0.26992\omega^2)(1 - \sqrt{T/T_c})]^2 \tag{5}$$

where T_c, P_c, and ω are the critical temperature, the critical pressure, and the acentric factor, respectively.

Modern EoS methods include an excess Gibbs free energy (G^E) model in the mixing rules of the EoS [39]. This means that an activity coefficient model is used to describe the complex liquid phase, and the fugacity coefficient is calculated using a simple EoS. Thus, the connection between the EoS and the G^E seems to be the most appropriate for modeling complex mixtures [38]. In this work, as one of those types of mixing rules, we used the Wong-Sandler (WS) mixing rule [39,40], which could be expressed as follows:

$$b = \frac{\sum_i \sum_j x_i x_j \left(b - \frac{a}{RT}\right)_{ij}}{1 - \left[\sum_i x_i \frac{a_i}{b_i RT} + \frac{G_0^E}{CRT}\right]} \tag{6}$$

and

$$a = b\left[\sum_i^N x_i \frac{a_i}{b_i} + \frac{G_0^E}{C}\right] \tag{7}$$

with the combining rule:

$$\left(b - \frac{a}{RT}\right)_{ij} = \frac{1}{2}(b_i + b_j) - \frac{\sqrt{a_i a_j}}{RT}(1 - k_{ij}) \tag{8}$$

Table 2. Critical properties and acentric factor estimated for ionic liquids

Ionic liquid	Critical temperature, T_c (K)	Critical pressure, P_c (MPa)	Critical compressibility factor, Z_c	Acentric factor, ω
[bmpyr][dca]	988.3	2.13	0.194	0.832
[bmpyr][Tf_2N]	1209.2	2.48	0.254	0.319
CO_2	304.2	7.38	0.274	0.224

In these equations, a and b are the EoS parameters of the mixture in ionic liquid phase. k_{ij} is an adjustable binary interaction parameter, which is dependent of temperature. a_i and b_i are the EoS parameters for pure component i, which are calculated by Eqs. (3) to (5). G_0^E is the molar excess Gibbs free-energy obtained from any excess free-energy model. The C term is the EoS-dependent constant: $C=\ln(\sqrt{2}-1)/\sqrt{2}\approx-0.62323$ for the PR-EoS.

We calculated the excess Gibbs free energy G_0^E in the mixing rules using the van Laar equation [37]:

$$\frac{G_0^E}{RT}=\frac{A_{12}A_{21}x_1x_2}{A_{12}x_1+A_{21}x_2} \tag{9}$$

where A_{12}, A_{21} are the model parameters. The van Laar equation has been shown to perform well in high pressure phase equilibrium calculations [38]. Consequently, in our phase equilibrium calculations, the model parameters are the k_{12} parameter in the combining rule and the two parameters (A_{12}, A_{21}) in the van Laar equation used to calculate the excess Gibbs free-energy.

The expressions for the fugacity coefficients of CO_2 (component 1) in the gas phase and in the ionic liquid phase using the PR-EoS and the WS mixing rules are as follows:

$$\ln\phi_1^{gas}=\ln\frac{f_1^{gas}}{P}=(Z^{gas}-1)-\ln\left(Z^{gas}-\frac{b_1}{RT}\right)-\frac{a_1}{2\sqrt{2}b_1RT}\ln\left[\frac{Z^{gas}+(1+\sqrt{2})(b_1/RT)}{Z^{gas}+(1-\sqrt{2})(b_1/RT)}\right] \tag{10}$$

and

$$\ln\hat{\phi}_1^{IL}=\ln\frac{\hat{f}_1^{IL}}{x_1P}=\frac{1}{b}\left[\frac{\partial(nb)}{\partial n_1}\right]_{T,n_2}(Z^{IL}-1)-\ln\left(Z^{IL}-\frac{b}{RT}\right)-\frac{a}{2\sqrt{2}bRT}\left\{\frac{1}{an}\left[\frac{\partial(n^2a)}{\partial n_1}\right]_{T,n_2}-\frac{1}{b}\left[\frac{\partial(nb)}{\partial n_1}\right]_{T,n_2}\right\}\ln\left[\frac{Z^{IL}+(1+\sqrt{2})(b/RT)}{Z^{IL}+(1-\sqrt{2})(b/RT)}\right] \tag{11}$$

Note that in Eqs. (10) and (11), $Z^{gas}=PV^{gas}/(RT)$ and $Z^{IL}=PV^{IL}/(RT)$. The partial derivative terms in Eq. (11) are as follows:

$$\left[\frac{\partial(nb)}{\partial n_1}\right]_{T,n_2}=\frac{1}{1-D}\frac{1}{n}\left[\frac{\partial(n^2q)}{\partial n_1}\right]_{T,n_2}-\frac{q}{(1-D)^2}\left\{1-\left[\frac{\partial(nD)}{\partial n_1}\right]_{T,n_2}\right\} \tag{12}$$

and

$$\frac{1}{n}\left[\frac{\partial(n^2a)}{\partial n_1}\right]_{T,n_2}=RT\left\{D\left[\frac{\partial(nb)}{\partial n_1}\right]_{T,n_2}+b\left[\frac{\partial(nD)}{\partial n_1}\right]_{T,n_2}\right\} \tag{13}$$

where, $q=\sum_i\sum_j x_ix_j\left(b-\frac{a}{RT}\right)_{ij}$, $D=\sum_i x_i\frac{a_i}{b_iRT}+\frac{G_0^E}{CRT}$, $\frac{1}{n}\left[\frac{\partial(n^2q)}{\partial n_1}\right]_{T,n_2}=2\sum_j x_j\left(b-\frac{a}{RT}\right)_{1j}$, and $\left[\frac{\partial(nD)}{\partial n_1}\right]_{T,n_2}=\frac{a_1}{b_1RT}+\frac{\ln\gamma_1}{C}$.

The use of the PR-EoS requires information on the critical properties and acentric factor for each component of the binary system. Those properties are readily available for CO_2, while they are not available for ionic liquids. Therefore, those properties for ionic liquids have to be estimated. We used the modified Lydersen-Joback-Reid group contribution method proposed by Valderrama et al. [41] to estimate the critical temperature and pressure and the acentric factor of the ionic liquids studied. The estimated values of the properties for the ionic liquids studied in this work are given in Table 2 along with those for CO_2.

The phase equilibrium calculation for the CO_2+ionic liquid system was performed in the following way. At a given temperature, equilibrium pressures (P) satisfying Eq. (1) were calculated as a function of CO_2 mole fraction (x_1). The volumetric properties of CO_2 and ionic liquid phases, which were required to calculate f_1^{gas} and $\hat{f}_1^{IL}$, were obtained by solving Eq. (2). A nonlinear least square method was used to perform this calculation [42,43]. The same calculations were repeated at different temperatures.

A set of the optimum values of the three parameters (k_{12}, A_{12}, and A_{21} in Eqs. (8) and (9)) at each temperature for a binary system was determined first before performing the above phase equilibrium calculation. Those values were obtained by correlating the experimental $P-x_1$ data with the PR-EoS and minimizing the following objective function:

$$F=\sum_{m=1}^{N}\frac{\left|P_m^{calc}-P_m^{exp}\right|}{P_m^{exp}} \tag{14}$$

where P_m^{exp} is the experimental value of equilibrium pressure for data point m, P_m^{calc} is the equilibrium pressure calculated by the PR-EoS at the experimental value of x_1 for the same data point, and N is the number of data points. An optimization routine, which solved a nonlinear least-squares problem, was used [43].

RESULTS AND DISCUSSION

1. CO_2 Solubility in [bmpyr]-based Ionic Liquids

Tables 3 and 4 show the experimental results of the phase boundaries for two binary systems: CO_2+[bmpyr][dca] and CO_2+[bmpyr][Tf_2N], respectively. In those tables, the equilibrium pressures observed at the bubble or cloud point of the CO_2 (component 1)+ ionic liquid (component 2) mixtures with different CO_2 mole fractions are given in the temperature range from about 303 K to about 343 K. The solubilities of CO_2 in the ionic liquid phase are represented in terms of two units: the mole fraction (x_1) based on the moles of CO_2 and ionic liquids; and the molality (m_1) based on

Table 3. Experimental bubble or cloud point data for various mole fractions of CO_2 in the CO_2+[bmpyr][dca] system

Mole fraction of CO_2, x_1	Uncertainty in x_1	Molality, m_1 (mol of CO_2/kg of ionic liquid)	T (K)	P (MPa)	Phase behavior observed
0.1097	0.0028	0.5918	303.7	0.42	b*
			313.5	0.53	b
			322.5	0.64	b
			332.8	0.79	b
			343.4	0.92	b
0.1703	0.0039	0.9855	303.1	0.80	b
			312.7	0.92	b
			324.1	1.17	b
			333.8	1.42	b
			343.3	1.63	b
0.2176	0.0049	1.3348	303.0	1.08	b
			313.7	1.40	b
			323.1	1.69	b
			333.7	2.07	b
			342.8	2.42	b
0.2479	0.0060	1.5825	303.2	1.49	b
			312.6	1.84	b
			322.7	2.26	b
			333.6	2.78	b
			343.1	3.28	b
0.3128	0.0066	2.1847	303.9	2.26	b
			313.1	2.79	b
			323.2	3.43	b
			333.1	4.13	b
			343.0	4.89	b
0.3832	0.0071	2.9825	303.9	2.95	b
			313.5	3.68	b
			322.4	4.41	b
			333.0	5.43	b
			342.8	6.48	b
0.4326	0.0076	3.6603	303.7	3.64	b
			313.2	4.54	b
			321.7	5.45	b
			332.2	6.72	b
			343.0	8.16	b
0.4723	0.0081	4.2964	303.2	4.32	b
			312.2	5.37	b
			322.5	6.78	b
			332.4	8.41	b
			342.2	10.18	b
0.5216	0.0083	5.2350	302.6	5.34	b
			312.2	6.89	b
			322.5	9.02	b
			333.7	11.91	b
			342.6	14.84	b

the mass of ionic liquid. The CO_2 solubility data in both units are listed in Tables 3 and 4. The uncertainty in the solubility measurement is also given for each point. The average uncertainty value in x_1 was estimated to be 0.0061 for the CO_2+[bmpyr][dca] system and 0.0088 for the CO_2+[bmpyr][Tf_2N] system.

Solubility of gases including CO_2 in liquids tends to increase in

Table 3. Continued

Mole fraction of CO_2, x_1	Uncertainty in x_1	Molality, m_1 (mol of CO_2/kg of ionic liquid)	T (K)	P (MPa)	Phase behavior observed
0.5642	0.0085	6.2152	303.2	6.57	b
			311.7	8.72	b
			322.2	13.53	c**
			331.8	18.06	c
			342.0	22.83	c
0.6019	0.0086	7.2581	303.6	9.48	c
			312.7	14.99	c
			322.5	20.75	c
			332.4	26.21	c
			342.1	31.28	c

*Bubble point behavior observed
**Cloud point behavior observed

Table 4. Experimental bubble or cloud point data for various mole fractions of CO_2 in the CO_2+[bmpyr][Tf_2N] system

Mole fraction of CO_2, x_1	Uncertainty in x_1	Molality, m_1 (mol of CO_2/kg of ionic liquid)	T (K)	P (MPa)	Phase behavior observed
0.1423	0.0028	0.3927	303.3	0.39	b*
			312.8	0.47	b
			322.2	0.53	b
			332.0	0.63	b
			342.0	0.76	b
0.2378	0.0051	0.7387	302.7	0.92	b
			312.3	1.09	b
			322.0	1.28	b
			331.8	1.45	b
			341.5	1.67	b
0.3239	0.0070	1.1341	303.2	1.41	b
			312.0	1.64	b
			321.9	1.96	b
			332.0	2.26	b
			341.7	2.54	b
0.3891	0.0086	1.5076	302.8	1.85	b
			312.5	2.21	b
			322.1	2.57	b
			331.9	2.97	b
			341.9	3.47	b
0.4847	0.0094	2.2270	302.8	2.62	b
			312.5	3.13	b
			322.4	3.73	b
			331.8	4.34	b
			342.7	5.16	b
0.5501	0.0101	2.8943	302.8	3.31	b
			312.0	3.98	b
			322.0	4.79	b
			331.8	5.70	b
			342.4	6.75	b

proportion to pressure or decrease in inverse proportion to temperature. This tendency is universally applied to most ionic liquids reliant on physical absorption [9-26]. Even in chemical absorption with a strong CO_2 absorption capacity, dependence on physical

Table 4. Continued

Mole fraction of CO_2, x_1	Uncertainty in x_1	Molality, m_1 (mol of CO_2/kg of ionic liquid)	T (K)	P (MPa)	Phase behavior observed
			302.7	4.32	b
			312.7	5.34	b
0.6199	0.0103	3.8609	322.4	6.47	b
			332.2	7.81	b
			341.8	9.17	b
			302.9	5.33	b
			312.7	6.67	b
0.6722	0.0104	4.8549	322.0	8.19	b
			331.8	10.08	b
			342.3	12.34	b
			303.1	6.29	b
			311.9	7.92	b
0.7125	0.0104	5.8682	322.3	10.49	b
			332.0	13.53	b
			341.7	16.64	b
			302.9	6.73	b
			312.3	9.24	b
0.7444	0.0105	6.8952	323.7	13.58	b
			331.8	16.64	b
			341.9	20.36	b
			302.7	10.88	c**
			312.4	15.67	c
0.7761	0.0102	8.2078	321.8	20.16	c
			331.7	24.42	c
			341.5	28.47	c

*Bubble point behavior observed
**Cloud point behavior observed

absorption appears after absorption of a certain amount of CO_2. Our studies for two [bmpyr] cation-based ionic liquids confirmed this trend as well.

For each data point, information on the phase change behavior observed during measurement, i.e., bubble or cloud point behavior, is also given in Tables 3 and 4. As indicated in the tables, the cloud point behavior rather than the bubble point behavior was observed for solutions of quite high CO_2 mole fractions. The CO_2 mole fraction at which the cloud point behavior was observed depended on the system. This phenomenon can be explained in the following manner, as already discussed in our previous publication [13]. When the CO_2 solubility in ionic liquid is measured in our experiments, the pressure is slowly reduced until the phase separation occurs from the single-phase solution where CO_2 is dissolved in the ionic liquid phase. When the CO_2 mole fraction in the solution is small and the equilibrium pressure is low, CO_2 behaves like a gas, and thus the tiny bubbles come out of the solution with the pressure decrease even at temperatures above the critical point of CO_2. However, at higher CO_2 mole fractions and higher pressure, CO_2 behaves like a liquid, and the cloud pressure behavior is observed with a decrease of the equilibrium pressure. It is acknowledged that the high density of the CO_2 phase makes the demixing appear closer to liquid-liquid equilibrium behavior than to vapor-liquid equilibrium behavior. Due to the phase transition from a single phase to a liquid+liquid phase, the solution becomes cloudy at the cloud point. The cloud point behavior was observed when the sharp increase of equilibrium pressure with the increase of CO_2 solubility occurred.

The graphical presentations of the experimental data are shown in Fig. 2 for both systems in the form of P−T isopleths. At a given CO_2 mole fraction, the equilibrium pressure increased as temperature increased. The change of the equilibrium pressure with respect to temperature increased with the increase of the CO_2 mole fraction. The isothermal variation of the CO_2 solubility with respect to the equilibrium pressure at a fixed temperature was more distinctly observed from the x_1–P (or the m_1–P) isotherms generated by plotting x_1 (or m_1) as a function of P at various temperatures. For this purpose, first, the data of the P−T curves in Fig. 2 were fitted with polynomial equations (second- or third-order) to obtain the curve fits. And then the equilibrium pressures equivalent to desired temperatures were calculated from the curve fits. Finally, the CO_2 solubilities (x_1 and m_1) as a function of the equilibrium pressure (P) at five different temperatures from 303.2 K to 343.2 K with an interval of 10 K were obtained for each system. The interpolated iso-

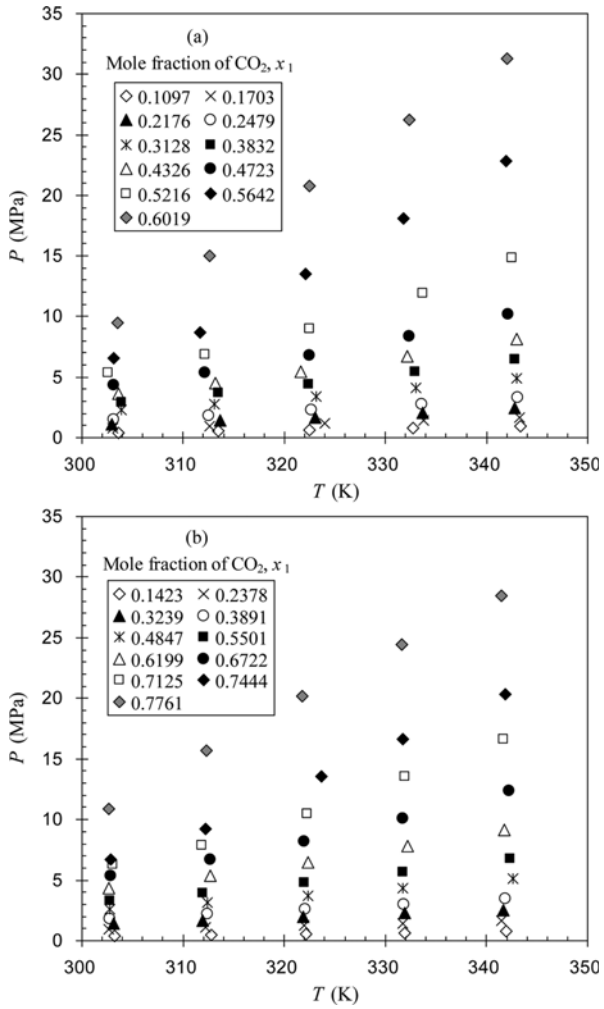

Fig. 2. P–T isopleths of phase boundaries for the CO_2+ionic liquid mixtures with various CO_2 mole fractions (x_1): (a) [bmpyr][dca]; (b) [bmpyr][Tf_2N].

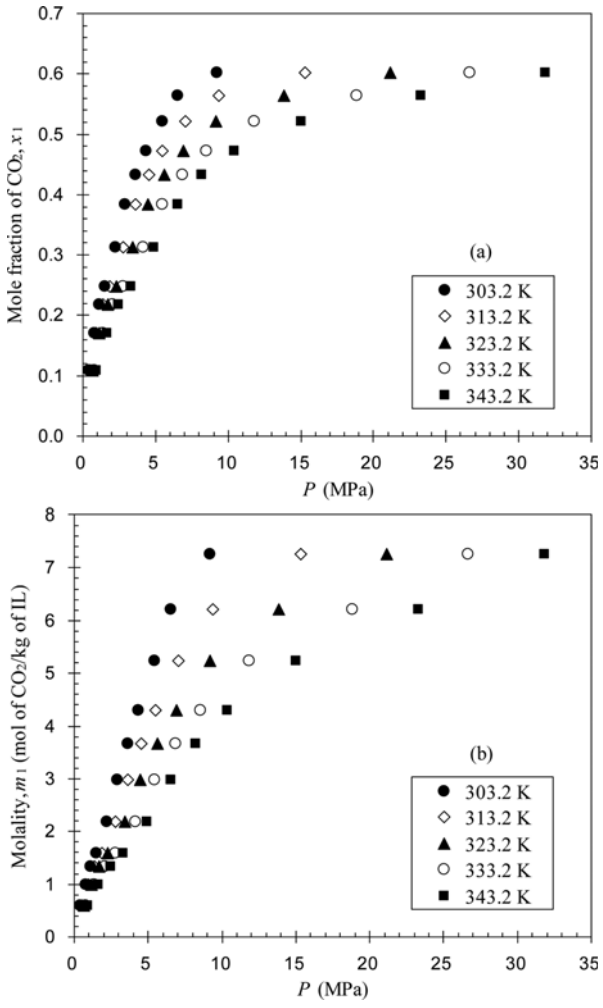

Fig. 3. CO_2 solubility in [bmpyr][dca] ionic liquid as a function of pressure at different temperatures: (a) in mole fraction; (b) in molality.

thermal x_1–P (and m_1–P) data obtained in this manner are listed in Table 5 for two systems, and graphical illustrations for those data are given in Figs. 3 and 4.

As shown in Figs. 3(a) and 4(a), the mole fraction of CO_2 dis-

Table 5. Interpolated isothermal solubility data for CO_2 in ionic liquids

Mole fraction of CO_2, x_1	Molality, m_1 (mol of CO_2/kg of ionic liquid)	P (MPa) at following temperature				
		303.2 K	313.2 K	323.2 K	333.2 K	343.2 K
Ionic liquid: [bmpyr][dca]						
0.1097	0.5918	0.41	0.53	0.65	0.78	0.92
0.1703	0.9855	0.79	0.95	1.15	1.38	1.64
0.2176	1.3348	1.09	1.38	1.70	2.05	2.44
0.2479	1.5825	1.49	1.86	2.28	2.76	3.29
0.3128	2.1847	2.22	2.79	3.43	4.14	4.91
0.3832	2.9825	2.91	3.64	4.49	5.45	6.52
0.4326	3.6603	3.59	4.54	5.62	6.84	8.19
0.4723	4.2964	4.32	5.50	6.90	8.53	10.38
0.5216	5.2350	5.44	7.04	9.17	11.83	15.01
0.5642	6.2152	6.54	9.39	13.86	18.86	23.27
0.6019	7.2581	9.22	15.32	21.13	26.63	31.84

Table 5. Continued

Mole fraction of CO_2, x_1	Molality, m_1 (mol of CO_2/kg of ionic liquid)	P (MPa) at following temperature				
		303.2 K	313.2 K	323.2 K	333.2 K	343.2 K
Ionic liquid: [bmpyr][Tf_2N]						
0.1423	0.3927	0.39	0.46	0.54	0.65	0.77
0.2378	0.7387	0.93	1.11	1.29	1.49	1.70
0.3239	1.1341	1.40	1.69	1.99	2.29	2.59
0.3891	1.5076	1.87	2.22	2.61	3.05	3.53
0.4847	2.2270	2.64	3.17	3.77	4.45	5.20
0.5501	2.8943	3.34	4.07	4.90	5.82	6.84
0.6199	3.8609	4.36	5.40	6.59	7.92	9.40
0.6722	4.8549	5.36	6.75	8.41	10.35	12.56
0.7125	5.8682	6.26	8.28	10.79	13.78	17.25
0.7444	6.8952	6.67	9.85	13.30	17.01	20.99
0.7761	8.2078	11.13	16.09	20.74	25.09	29.13

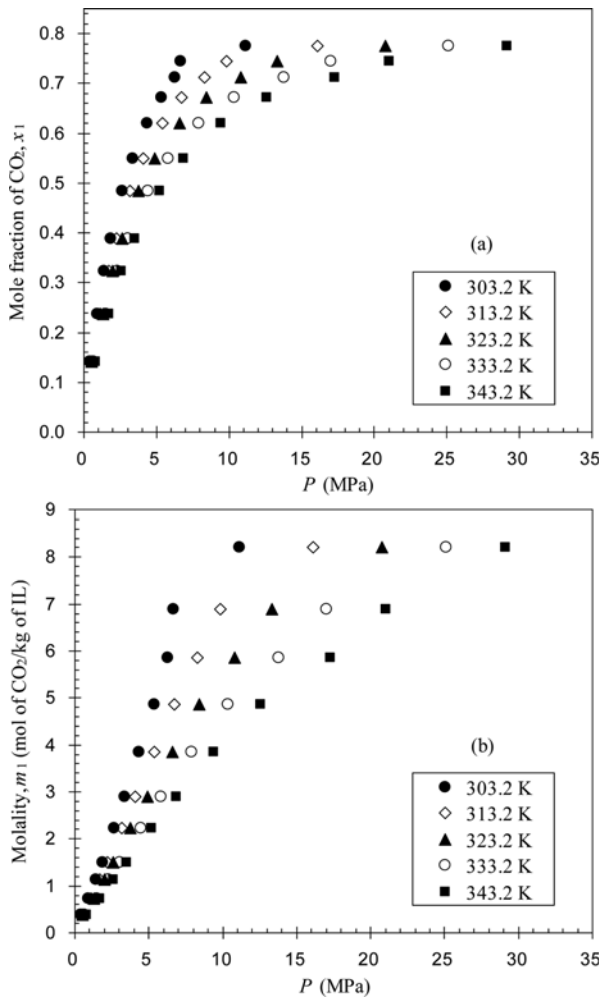

Fig. 4. CO_2 solubility in [bmpyr][Tf_2N] ionic liquid as a function of pressure at different temperatures: (a) in mole fraction; (b) in molality.

solved in the ionic liquid at a given temperature increased rapidly with increasing pressure while from about 10 MPa the rate of increase in the mole fraction decreased. Although there were some differences depending on the temperature, the CO_2 mole fraction almost reached saturation around 0.65 for [bmpyr][dca] and around 0.8 for [bmpyr][Tf_2N], respectively. In addition, the CO_2 solubility decreased with an isobaric increase in temperature. Larger temperature dependence was also observed at higher CO_2 solubilities. As the ionic liquids subject to this study basically show a phenomenon of physical absorption with regard to CO_2, the CO_2 mole fraction did not change significantly by a big increase in pressure at the pressures more than a particular pressure (for example, 10 MPa). Therefore, when CO_2 is dissolved in the ionic liquid phase, there seems to be a limitation the CO_2 solubility, which is also a limitation of physical absorption. Figs. 3(b) and 4(b) show the change of the CO_2 solubility based on the molality with the change of pressure at five different temperatures. At pressures smaller than about 10 MPa, the molality of CO_2 increased almost linearly with the increase of pressure. However, the rate of increase in the molality was reduced at higher pressures.

2. Comparison of CO_2 Solubility

Data comparisons on the CO_2 solubility in ionic liquids should be conducted with care. Many factors affect the experimental results, such as experimental methodology, sample source, sample purity, and so forth. Therefore, a direct comparison of experimental results from different research groups may be dangerous. This is especially true when compared at lower pressure regions, because the solubility differences are not so big. Note that most of the CO_2 solubility data for the ionic liquids compared in this work have been measured in our laboratory using the same experimental methodology. Thus, a direct comparison of data is possible.

Fig. 5(a) shows the comparison of the CO_2 solubility data at 323.2 K for the ionic liquids composed of [bmpyr] cation and various types of anions: [dca], [Tf_2N] and [TfO] (trifluoromethanesulfonate). The effect of anions constituting the ionic liquids on the CO_2 solubilities can be discussed from the results of Fig. 5(a). Compared at the same temperature and pressure, [bmpyr][Tf_2N] resulted in the highest CO_2 solubility. The CO_2 solubilities for [bmpyr][dca] and [bmpyr][TfO] were comparable. The relatively higher solubility of CO_2 in the [bmpyr][Tf_2N] ionic liquid may be due to favor-

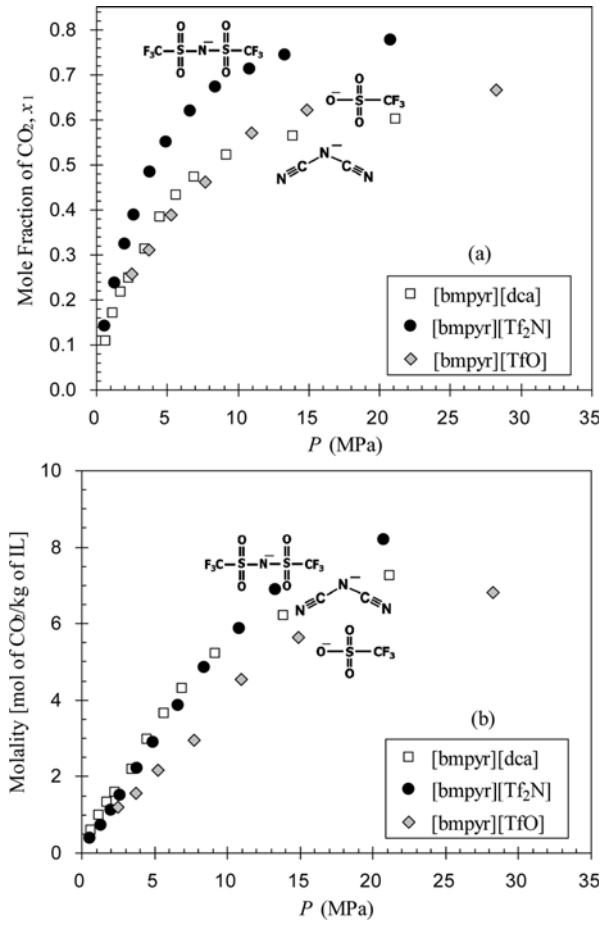

Fig. 5. Comparison of CO_2 solubility in [bmpyr] cation-based ionic liquids with different anions at 323.2 K: (a) solubility in mole fraction; (b) solubility in molality. The data for [bmpyr][TfO] are from reference [19].

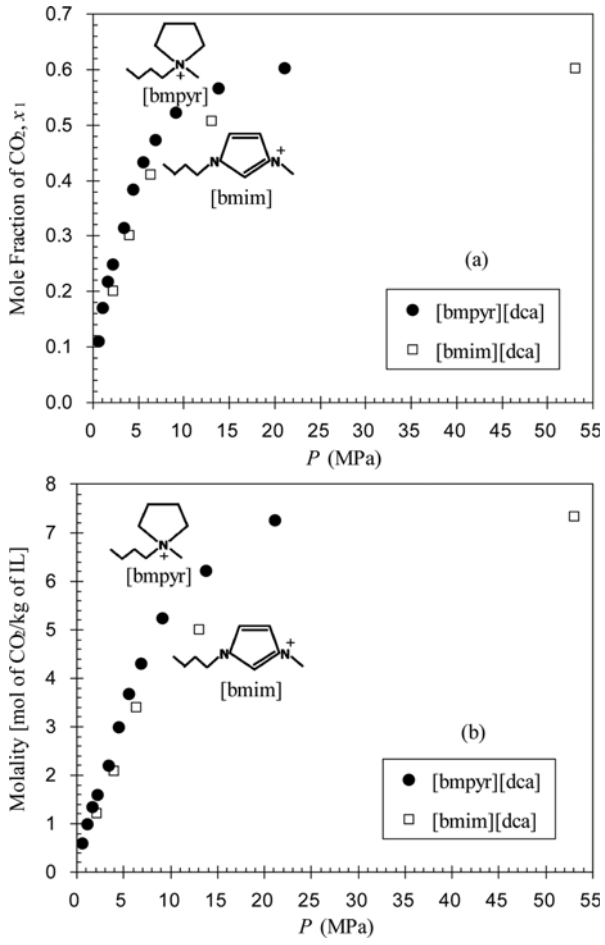

Fig. 6. Comparison of CO_2 solubility in ionic liquids [bmpyr][dca] and [bmim][dca] at 323.2 K: (a) solubility in mole fraction; (b) solubility in molality. The data for [bmim][dca] are from reference [14].

able interactions between CO_2 and the fluoroalkyl substituent (CF_3) on the anion. In Fig. 5(b), the CO_2 solubility data in three [bmpyr]-based ionic liquids are illustrated in terms of the molality instead of the mole fraction. Unlike the mole fraction data, the molality data showed a little different behavior. It was observed that the CO_2 solubilities in [bmpyr][dca] in terms of the molality were comparable to those in [bmpyr][Tf_2N], particularly at pressures lower than about 10 MPa. This can be attributed to the big difference in the molecular masses of [bmpyr][dca] and [bmpyr][Tf_2N]. Note that the molality is based on the mass of the solvent (ionic liquid). The [bmpyr][TfO] ionic liquid was observed to have the lowest CO_2 molalities.

Fig. 6 compares the CO_2 solubility data at 323.2 K for the ionic liquids: [bmpyr][dca] and [bmim][dca]. The [bmim], which stands for 1-butyl-3-methylimidazolium, is an imidazolium-based cation. It illustrates the effect of cation on the CO_2 solubility for the [dca] anion-based ionic liquids. Compared at the same temperature and pressure, [bmpyr][dca] had a higher CO_2 solubility than [bmim][dca], with respect to both the mole fraction and the molality. It indicates that CO_2 is more soluble in the pyrrolidinium-based ionic liquid than in the imidazolium-based ionic liquid.

Fig. 7 shows the comparison of the CO_2 solubility at 323.2 K for the [Tf_2N] anion-based ionic liquids with three different cations: [bmpyr], [bmim] and [bmpip]. The [bmpip], which denotes 1-butyl-1-methylpiperidinium, is a piperidinium-based cation. Note that the total length of the side chains attached to the main cation structure is the same for those three cations. As shown in Fig. 7, it is interesting that the CO_2 solubilities in those three ionic liquids did not give any distinct differences, with respect to both the mole fraction and the molality. Particularly, at lower pressure region, the CO_2 solubilities were almost the same. This phenomenon can be explained as follows. The anion in the ionic liquid turned out to play an essential role in determining the CO_2 solubility [9]. In general, higher solubilities of CO_2 are observed in ionic liquids with the [Tf_2N] anion, due to favorable interactions between CO_2 and the CF_3 substituent in the [Tf_2N] anion. Thus, for the ionic liquids with the [Tf_2N] anion, the effect of the anion on the CO_2 solubility is predominant, so the cation has little influence on the solubility of CO_2 for the ionic liquids with the [Tf_2N] anion. This is the reason why three ionic liquids shown in Fig. 7 gave almost the same solubilities for CO_2. There is one more point to be emphasized regarding the comparison of the CO_2 solubility data in ionic liquids. When comparing the solubility of CO_2 in ionic liquids, it is necessary to express

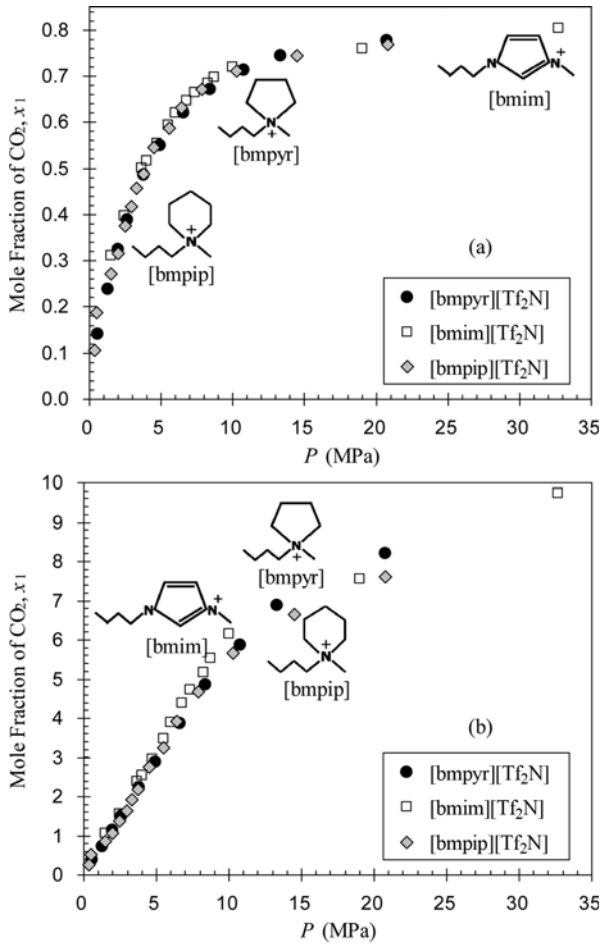

Fig. 7. Comparison of CO_2 solubility in [Tf_2N] anion-based ionic liquids with different cations at 323.2 K: (a) solubility in mole fraction; (b) solubility in molality. The data for [bmim][Tf_2N] and [bmpip][Tf_2N] are from references [12] and [27], respectively.

the CO_2 solubility in terms of the molality as well as the mole fraction: there may be a big difference in the molecular masses of ionic liquids depending on the types of cation and anion constituting the ionic liquids.

3. Correlation Results

The PR-EoS coupled with the WS mixing rules was used to correlate the experimental data of the solubility of CO_2 in the ionic liquids studied in this work. For each system of CO_2+ionic liquid, the three model parameters (k_{12}, A_{12}, and A_{21}) were optimized using the x_1−P data given in Table 5. Table 6 lists the optimum values of the model parameters at five different temperatures for each system. The parameter values given in Table 6 were fitted with the quadratic equations of Eqs. (15) to (17) with respect to temperature, and the results are shown in Table 7 for both the CO_2+ionic liquid systems.

$$k_{12} = k_{12,0} + k_{12,1}\left(\frac{T}{T_0}\right) + k_{12,2}\left(\frac{T}{T_0}\right)^2 \quad (15)$$

$$A_{12} = A_{12,0} + A_{12,1}\left(\frac{T}{T_0}\right) + A_{12,2}\left(\frac{T}{T_0}\right)^2 \quad (16)$$

Table 6. Model parameters and correlation results using the PR-EoS with the WS mixing rules for the CO_2+ionic liquid systems

Ionic liquid	T (K)	Model parameters			AAD%*
		k_{12}	A_{12}	A_{21}	
[bmpyr][dca]	303.2	0.7768	−1.4505	−0.3332	2.27
	313.2	0.9340	−1.0676	−0.3629	4.02
	323.2	1.1253	−0.8714	−0.4436	4.77
	333.2	1.4016	−0.7249	−0.6958	6.34
	343.2	1.8856	−0.6716	−2.1322	6.82
	Average				4.84
[bmpyr][Tf_2N]	303.2	0.3259	−1.0667	−0.6111	3.20
	313.2	0.3462	−1.0273	−0.6859	4.07
	323.2	0.3750	−0.9842	−0.7828	4.18
	333.2	0.4234	−0.8792	−0.9322	3.85
	343.2	0.4936	−0.8211	−1.1460	3.28
	Average				3.72

*Average absolute deviation in percentage, which is defined as:

$$AAD\% = \frac{1}{N}\sum_{m=1}^{N}\frac{\left|P_m^{calc} - P_m^{exp}\right|}{P_m^{exp}} \times 100 \quad \text{(N: number of data)}$$

Table 7. Coefficients of Eqs. (15) to (17) obtained for the CO_2+ionic liquid systems

Equation	Coefficients	Ionic liquid	
		[bmpyr][dca]	[bmpyr][Tf_2N]
(15)	$k_{12,0}$	47.5524	7.9476
	$k_{12,1}$	−93.6880	−15.2017
	$k_{12,2}$	46.9133	7.5801
	R^2	0.9960	0.9990
(16)	$A_{12,0}$	−59.8669	4.3808
	$A_{12,1}$	103.2257	−11.7799
	$A_{12,2}$	−45.0062	6.3138
	R^2	0.9966	0.9845
(17)	$A_{21,0}$	−210.3078	−21.1742
	$A_{21,1}$	399.1184	41.5492
	$A_{21,2}$	−189.5276	−20.9778
	R^2	0.9398	0.9990

$$A_{21} = A_{21,0} + k_{21,1}\left(\frac{T}{T_0}\right) + k_{21,2}\left(\frac{T}{T_0}\right)^2 \quad (17)$$

Note that T is in K and T_0=298.15 K.

The calculated results are graphically presented in Fig. 8 along with the experimentally obtained data of Table 5. The correlation results are summarized in Table 6. The average absolute deviations in percentage (AAD%) between the calculated and experimental equilibrium pressures were calculated at the five temperatures for each system. The average value of AAD% for entire data points in the whole range of temperature was 4.84% for [bmpyr][dca] and 3.72% for [bmpyr][Tf_2N], respectively. The CO_2+[bmpyr][Tf_2N] system gave a somewhat better correlation result. Overall, it can be concluded that the PR-EoS coupled with the WS mixing rules can satisfactorily correlate the high-pressure solubility of CO_2 in [bmpyr][dca] and [bmpyr][Tf_2N] with the AAD% less than 5% over a wide

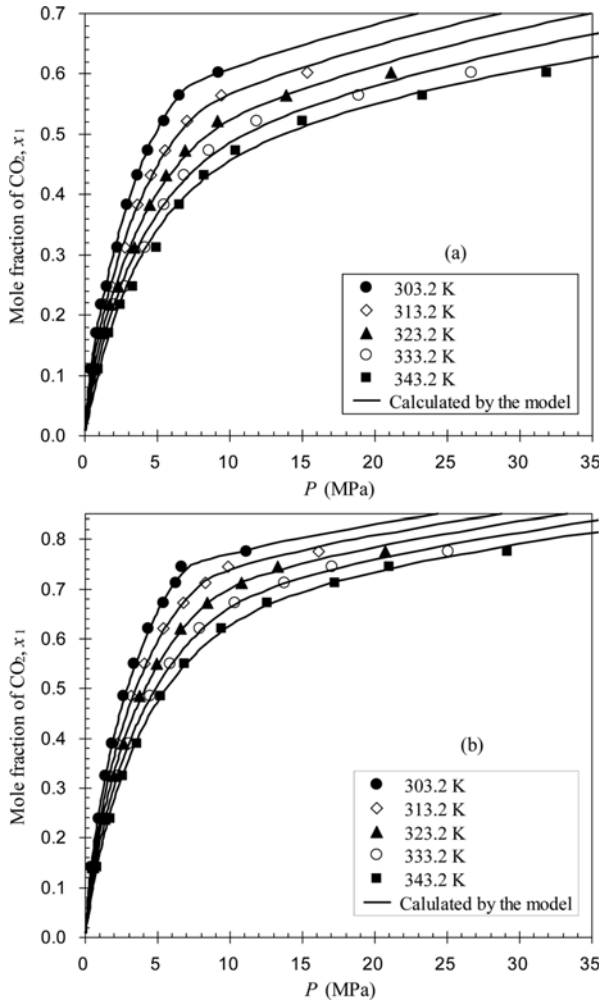

Fig. 8. Comparison between experimental values and calculated results by the PR-EoS with the WS mixing rules for CO_2 solubility in ionic liquids: (a) [bmpyr][dca]; (b) [bmpyr][Tf_2N].

range of pressure up to the supercritical region of CO_2.

CONCLUSIONS

For two kinds of pyrrolidinium-based ionic liquids with different anions ([bmpyr][dca][and [bmpyr][Tf_2N]], their solubilities of CO_2 were determined by measuring the bubble or cloud point pressures of the binary mixtures of CO_2+ionic liquid using a high-pressure equilibrium apparatus equipped with a variable-volume view cell. The CO_2 solubilities in the ionic liquids were discussed with respect to both the mole fraction and the molality. For both the ionic liquids, the solubilities of CO_2 increased with the increase of pressure and the decrease of temperature. To investigate the effect of the cation and the anion constituting the ionic liquid on the CO_2 solubility, our solubility data were compared with the data for other ionic liquids such as [bmpyr][TfO], [bmim][dca], [bmim][Tf_2N], and [bmpip][Tf_2N]. Compared at the same temperature and pressure, [bmpyr][Tf_2N] resulted in a higher CO_2 solubility than [bmpyr][TfO] and [bmpyr][dca]. [bmpyr][dca] had a higher CO_2 solubility than [bmim][dca], which indicated that CO_2 was more soluble in the pyrrolidinium-based ionic liquid than in the imidazolium-based ionic liquid. Three ionic liquids [bmpyr][Tf_2N], [bmim][Tf_2N] and [bmpip][Tf_2N] gave almost the same CO_2 solubilities with respect to both the mole fraction and the molality, since the effect of the anion on the CO_2 solubility was predominant for the ionic liquids with the [Tf_2N] anion. The solubility data of CO_2 in our two pyrrolidinium-based ionic liquids could be successfully correlated by using the Peng-Robinson equation of state coupled with the Wong-Sandler mixing rules over a wide range of pressure up to the supercritical region of CO_2. The average value of AAD% for entire data points in the whole range of temperature was 4.84% for [bmpyr][dca] and 3.72% for [bmpyr][Tf_2N], respectively.

ACKNOWLEDGEMENT

This research was supported by the 2014 Research Fund of Hannam University.

REFERENCES

1. M. Ramdin, T. W. de Loos and T. J. H. Vlugt, *Ind. Eng. Chem. Res.*, **51**, 8149 (2012).
2. R. S. Haszeldine, *Science*, **325**, 1647 (2009).
3. C. Gough, *Int. J. Greenhouse Gas Control*, **2**, 155 (2008).
4. G. T. Rochelle, *Science*, **325**, 1652 (2009).
5. P. D. Vaidya and E. Y. Kenig, *Chem. Eng. Technol.*, **30**, 1467 (2007).
6. H. Zhao, *Chem. Eng. Commun.*, **193**, 1660 (2006).
7. J. E. Bara, T. K. Carlisle, C. J. Gabriel, D. Camper, A. Finotello, D. L. Gin and R. D. Noble, *Ind. Eng. Chem. Res.*, **48**, 2739 (2009).
8. K. Kedra-Królik, F. Mutelet and J. N. Jaubert, *Ind. Eng. Chem. Res.*, **50**, 2296 (2011).
9. J. L. Anthony, J. L. Anderson, E. J. Maginn and J. F. Brennecke, *J. Phys. Chem. B*, **109**, 6366 (2005).
10. M. J. Muldoon, S. N. V. K. Aki, J. L. Anderson, J. K. Dixon and J. F. Brennecke, *J. Phys. Chem. B*, **111**, 9001 (2007).
11. J. Jacquemin, P. Husson, V. Majer and M. F. Costa-Gomes, *J. Solution Chem.*, **36**, 967 (2007).
12. E. K. Shin, B. C. Lee and J. S. Lim, *J. Supercrit. Fluids*, **45**, 282 (2008).
13. E. K. Shin and B. C. Lee, *J. Chem. Eng. Data*, **53**, 2728 (2008).
14. P. J. Carvalho, V. H. Alvarez, I. M. Marrucho, M. Aznar and J. A. P. Coutinho, *J. Supercrit. Fluids*, **50**(2), 105 (2009).
15 M. Hasib-ur-Rahman, M. Siaj and F. Larachi, *Chem. Eng. Processing*, **49**, 313 (2010).
16. F. Karadas, M. Atilhan and S. Aparicio, *Energy Fuels*, **24**, 5817 (2010).
17. W. Ren, B. Sensenich and A. M. Scurto, *J. Chem. Thermodyn.*, **42**, 305 (2010).
18. A. L. Revelli, F. Mutelet and J. N. Jaubert, *J. Phys. Chem. B*, **114**, 12908 (2010).
19. H. N. Song, B.-C. Lee and J. S. Lim, *J. Chem. Eng. Data*, **55**, 891 (2010).
20. J.-H. Yim, H. N. Song, B.-C. Lee and J. S. Lim, *Fluid Phase Equilib.*, **308**, 147 (2011).
21. J.-H. Yim, H. N. Song, K. P. Yoo and J. S. Lim, *J. Chem. Eng. Data*, **56**, 1197 (2011).
22. J.-Y. Jung and B.-C. Lee, *Anal. Sci. Technol.*, **24**(6), 467 (2011).
23. Y.-H. Jung, J.-Y. Jung, Y.-R. Jin, B.-C. Lee and I.-H. Baek, *J. Chem.*

Eng. Data, **57**, 3321 (2012).
24. S. G. Nam and B.-C. Lee, *Korean J. Chem. Eng.*, **30**(2), 474 (2013).
25. I. Mejia, K. Stanley, R. Canales and J. F. Brennecke, *J. Chem. Eng. Data*, **58**, 2642 (2013).
26. Z. Lei, C. Dai and B. Chen, *Chem. Rev.*, **114**, 1289 (2014).
27. S.-K. Nam and B.-C. Lee, *Anal. Sci. Technol.*, **27**(2), 79 (2014).
28. M. R. Ally, J. Braunstein, R. E. Baltus, S. Dai, D. W. DePaoli and J. M. Simonson, *Ind. Eng. Chem. Res.*, **43**, 1296 (2004).
29. X. Ji and H. Adidharma, *Fluid Phase Equilib.*, **293**, 141 (2010).
30. M. Yazdizadeh, F. Rahmani and A. A. Forghani, *Korean J. Chem. Eng.*, **28**(1), 246 (2011).
31. F. M. Maia, I. Tsivintzelis, O. Rodriguez, E. A. Macedo and G. M. Kontogeorgis, *Fluid Phase Equilib.*, **332**, 128 (2012).
32. Y. Chen, F. Mutelet and J.-N. Jaubert, *J. Phys. Chem. B*, **116**, 14375 (2012).
33. R. Macias-Salinas, J. A. Chavez-Velasco and M. A. Aquino-Olivos, *Ind. Eng. Chem. Res.*, **52**, 7593 (2013).
34. L. F. Vega, O. Vilaseca, F. Llovell and J. S. Andreu, *Fluid Phase Equilib.*, **294**, 15 (2010).
35. *Guide to the Expression of Uncertainty in Measurement*, International Organization of Standardization (ISO), Geneva, Switzerland (1995).
36. J. M. Lee, B.-C. Lee and S.-H. Lee, *J. Chem. Eng. Data*, **45**, 851 (2000).
37. J. M. Prausnitz, R. N. Lichtenthaler and E. G. de Azevedo, *Molecular Thermodynamics of Fluid-Phase Equilibria*, 3rd Ed., Prentice-Hall, NJ, USA (1999).
38. J. A. Lazzus, *Commun. Comput. Phys.*, **14**(1), 107 (2013).
39. H. Orbay and S. I. Sandler, *Modeling Vapor-Liquid Equilibria. Cubic Equations of State and Their Mixing Rules*, Cambridge University Press, UK (1998).
40. D. S. H. Wong and S. I. Sandler, *AIChE J.*, **38**, 671 (1992).
41. J. O. Valderrama, L. A. Forero and R. E. Rojas, *Ind. Eng. Chem. Res.*, **51**, 7838 (2012).
42. J. Winnick, *Chemical Engineering Thermodynamics*, Wiley, New York, NY, 451 (1997).
43. IMSL Math/Library: FORTRAN Subroutines for Mathematical Applications, Vol. 2, Visual Numerics, Inc. (1994).